Journal of Power Sources 196 (2011) 39–45

Contents lists available at ScienceDirect

Journal of Power Sources

journal homepage: www.elsevier.com/locate/jpowsour

New insights in the polarization resistance of anode-supported solid oxide fuel cells with $La_{0.6}Sr_{0.4}Co_{0.2}Fe_{0.8}O_3$ cathodes

Zigui Lu*, John Hardy, Jared Templeton, Jeffry Stevenson

Energy and Environmental Directorate, Pacific Northwest National Laboratory, K2-03, Richland, WA 99352, USA

ARTICLE INFO

Article history:
Received 18 May 2010
Received in revised form 17 July 2010
Accepted 20 July 2010
Available online 30 July 2010

Keywords:
LSCF cathode
Electrochemical impedance spectroscopy
Operating voltage
Tafel
Concentration polarization

ABSTRACT

In this study, the polarization resistance of anode-supported solid oxide fuel cells (SOFC) with $La_{0.6}Sr_{0.4}Co_{0.2}Fe_{0.8}O_3$ (LSCF) cathodes was investigated by *I–V* sweep and electrochemical impedance spectroscopy under a series of operating voltages and cathode environments (i.e. stagnant air, flowing air, and flowing oxygen) at temperatures from 550 °C to 750 °C. In flowing oxygen, the polarization resistance of the fuel cell decreased considerably with the applied current density. A linear relationship was observed between the ohmic-free over-potential and the logarithm of the current density of the fuel cell at all the measuring temperatures. In stagnant or flowing air, an arc related to the molecular oxygen diffusion through the majority species (molecular nitrogen) present in the pores of the cathode was identified at high temperatures and high current densities. The magnitude of this arc increased linearly with the applied current density due to the decreased oxygen partial pressure at the interface of the cathode and the electrolyte. It is found that the performance of the fuel cell in air is mainly determined by the oxygen diffusion process. Elimination of this process by flowing pure oxygen to the cathode improved the cell performance significantly. At 750 °C, for a fuel cell with a laser-deposited $Sm_{0.2}Ce_{0.8}O_{1.9}$ (SDC) interlayer, an extraordinarily high power density of 2.6 W cm^{-2} at 0.7 V was achieved in flowing oxygen, as a result of reduced ohmic and polarization resistance of the fuel cell, which were 0.06 Ω cm^2 and 0.03 Ω cm^2, respectively. The results indicate that microstructural optimization of the LSCF cathode or adoption of a new cell design which can mitigate the oxygen diffusion limitation in the cathode might enhance cell performance significantly.

Published by Elsevier B.V.

1. Introduction

Oxygen reduction at the cathode side of solid oxide fuel cells (SOFC) is a very complex process which involves the interaction of electronic, ionic, and molecular species. The overall oxygen reduction mechanism usually consists of several steps such as gas diffusion in the pores of the electrode, absorption, dissociation, and charge transfer at the gas/electrode interface, surface migration or bulk diffusion of oxygen ions through the electrode material, and the transfer of oxygen ions at the electrode/electrolyte interface. Numerous studies have been undertaken to investigate the reaction mechanism either by modeling or experiments. However, there is still a lot of work needed to reach a consensus in understanding the oxygen reduction mechanism due to the large number of variables involved, including the physico-chemical properties (e.g., ionic/electronic conductivities, oxygen diffusion coefficient, and electro-catalytic properties) and the microstructure (e.g., pore size and distribution) of the cathode, as well as the testing conditions. Several reviews have been given on the cathode reaction mechanisms of solid oxide fuel cells [1,2].

Electrochemical impedance spectroscopy (EIS) is a powerful technique that is widely used by the fuel cell community to investigate the reaction mechanism because it can separate different processes based on their relaxation times. However, interpretation of the results is not always easy. A number of impedance studies have been carried out to understand the oxygen reduction mechanism, either on symmetrical cells [3–5] or complete cells [6,7], porous cathode [5,8–12] or dense cathode [13,14], LSM [3,7,11] or other mixed ionic and electronic conductors (MIEC) [5,9,15] for intermediate temperature applications. However, almost all the impedance studies were performed at open circuit voltage (OCV), where the fuel cell is in a reversible state, with only a few performed under operating voltages or current densities [7,15].

When EIS is performed at OCV on a complete fuel cell, a very small current, usually of several mA, passes through the fuel cell as a sinusoidal signal, which means that the current could be positive at one time and negative at another time. As a result, during the impedance measurement the fuel cell alternatively works as a fuel cell and an electrolyzer, which does not represent the true working conditions of the cathode where relatively high cur-

* Corresponding author. Tel.: +1 509 375 2782; fax: +1 509 375 4448.
E-mail address: zigui.lu@pnl.gov (Z. Lu).

0378-7753/$ – see front matter. Published by Elsevier B.V.
doi:10.1016/j.jpowsour.2010.07.054

rent always flows out (electrons flow in) during operation. Wang et al. [15] argued that even for symmetrical cells with a cathode/electrolyte/cathode structure, in the presence of an applied current, the symmetrical cell is no longer symmetrical since the two cathodes are polarized differently. Therefore, the polarization resistance calculated simply by counting half of the measured polarization resistance does not truly represent the actual polarization resistance of the cathode. Our previous study [6] demonstrated that the polarization resistance of the LSCF cathode is a dynamic property which decreases with the current density of the fuel cell.

In this study, we try to shed further light on the cathode reaction mechanism under real working conditions by performing EIS under a series of operating voltages and cathode environments.

2. Experimental

Ni + YSZ anode-supported YSZ thin films were fabricated by a tape-casting and lamination process, described in more detail elsewhere [16]. The green tape was cut into discs, sintered at 1385 °C for 2 h, and subsequently creep-flattened at 1350 °C for 2 h. The flattened substrate, which was about 25 mm in diameter, consisted of three layers: bulk Ni + YSZ anode, active Ni + YSZ anode, and YSZ electrolyte. The thicknesses of the bulk anode, active anode, and electrolyte were 1 mm, 8 μm, and 10 μm, repectively. The active anode contained 50 vol.% of Ni and 50 vol.% of YSZ after reduction, while the bulk anode contained 40 vol.% of Ni and 60 vol.% YSZ to improve the mechanical strength of the substrate and match the coefficient of thermal expansion between the substrate and the YSZ electrolyte.

An $Sm_{0.2}Ce_{0.8}O_{1.9}$ (SDC, Praxair) interlayer was employed between the YSZ electrolyte and the cathode to block potential interdiffusion and chemical reaction between the two components. The SDC interlayer was applied by screen-printing SDC ink onto the YSZ electrolyte and sintering at 1200 °C for 2 h. The fired SDC layer was about 4 μm thick and contained about 25% porosity, measured from the weight and volume of this layer. $La_{0.6}Sr_{0.4}Co_{0.2}Fe_{0.8}O_3$ (LSCF, Praxair) was used as the cathode material. The as-received powder (d_{50} = 1.0 μm) was attrition milled to reduce the particle size to about 0.3 μm. The LSCF cathode was fabricated by screen-printing LSCF ink onto the SDC interlayer and sintering at 900 °C for 2 h. $La_{0.8}Sr_{0.2}CoO_3$ (LSC, in house) was screen-printed onto the LSCF and sintered at 850 °C for 2 h to serve as the cathode current collector. The cathode area, 2 cm^2 in this study unless otherwise specified, was used as the effective area of the fuel cells to calculate the power density and area specific resistance (ASR). All the inks used in this study had about 40 wt.% solids loading and were prepared by mixing solid powders with V-006 binder (Heraeus) on a three-roll mill. A fuel cell with a dense SDC interlayer was fabricated by pulsed-laser-deposition and tested for comparison. Detailed information on the fabrication of the dense SDC interlayer is described elsewhere [17]. The fabrication procedures for the LSCF cathode and LSC cathode current collector were the same as those of the fuel cells with screen-printed SDC interlayer, except that the cathode area was 1 cm^2.

Screen-printed Au grids with embedded Au gauze and NiO grids (reduced to Ni metal *in situ*) with embedded Ni gauze were used to collect current from the cathode and anode, respectively. The cells were sealed to alumina tubes using a glass seal, and *I–V* and impedance spectra were recorded using a Solartron 1470 Multistat coupled with a Solartron 1255 frequency response analyzer. Electrochemical impedance spectroscopy was performed under OCV or an operating voltage. When performed under an operating voltage, the cell was held at that voltage for 10 min before the impedance measurement was executed. Moist hydrogen with a flow rate of 200 sccm was supplied to the anode and three different conditions were tested for the cathode side: stagnant air, flowing air, and flowing oxygen with a flow rate of 500 sccm. After testing, the fuel cells were observed under scanning electron microscopy (SEM) (JEOLJSM-5900LV) for cross-sectional views.

3. Results and discussion

3.1. Microstructure of the LSCF cathode

Fig. 1 shows the cross-sectional SEM micrographs of a fuel cell with LSCF cathode sintered at 900 °C for 2 h and LSC current collector sintered at 850 °C for 2 h. The LSCF cathode and LSC current collector were each about 20 μm thick after sintering. The LSCF cathode showed a relatively dense structure with an average pore size under 1 μm, while the LSC current collector exhibited a more open structure, with pore sizes larger than 1 μm. Strong bonding between each layer was observed. It is noted that cracking at the interface of the YSZ electrolyte and the SDC interlayer most likely occurred during SEM sample preparation, due to the shrinking of the mounting resin.

3.2. Polarization resistance of the LSCF cathode

I–V sweep and electrochemical impedance spectroscopy (EIS) of the fuel cells were performed at 550 °C, 650 °C, and 750 °C under three different cathode conditions, i.e. stagnant air, flowing air, and flowing oxygen with a flow rate of 500 sccm. The EIS was performed under a series of operating voltages, which covered the entire range of voltages used in the *I–V* measurements. Figs. 2 and 3 give two examples of the *I–V* characteristics of a fuel cell tested at 750 °C and 550 °C, respectively, with the corresponding electrochemical

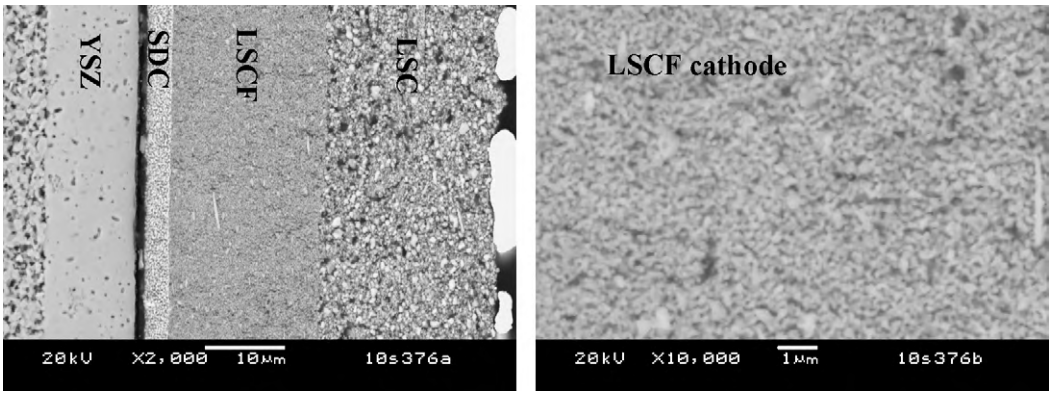

Fig. 1. Cross-sectional SEM micrographs of a fuel cell with LSCF cathode sintered at 900 °C for 2 h and LSC current collector sintered at 850 °C for 2 h.

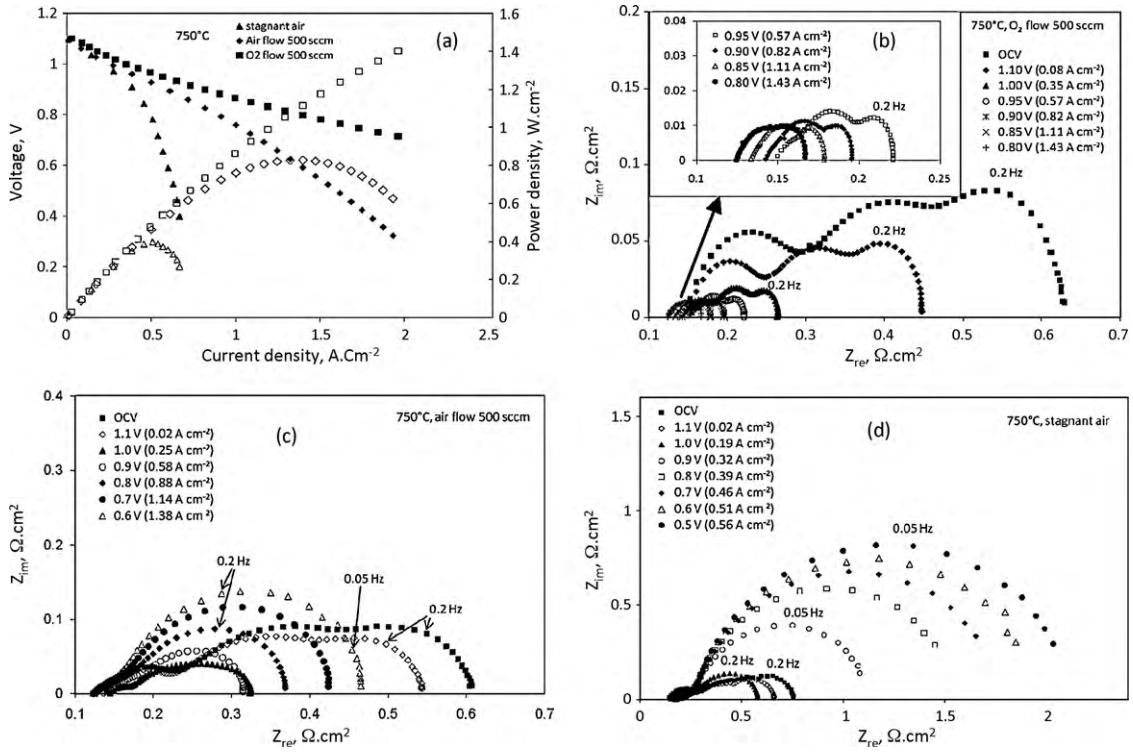

Fig. 2. *I–V* characteristics (a) and electrochemical impedance spectra (b–d) of a fuel cell tested at 750 °C in three different cathode environments.

impedance spectra also included. In the legend of Figs. 2 and 3, the current density corresponding to each applied voltage for the EIS measurements was also included in the parentheses following the applied voltage.

At 750 °C, the cell performance increased significantly in a sequence of stagnant air, flowing air, and flowing oxygen, as shown in Fig. 2a. The maximum power densities of the fuel cell were 0.4 W cm^{-2} and 0.8 W cm^{-2} in stagnant air and flowing air, respectively. The power density of the fuel cell was over 1.4 W cm^{-2} at 0.7 V in pure oxygen flow, with the maximum power density estimated to be over 1.8 W cm^{-2}. All the *I–V* curves had very similar slopes when the current density was small. However, the *I–V*

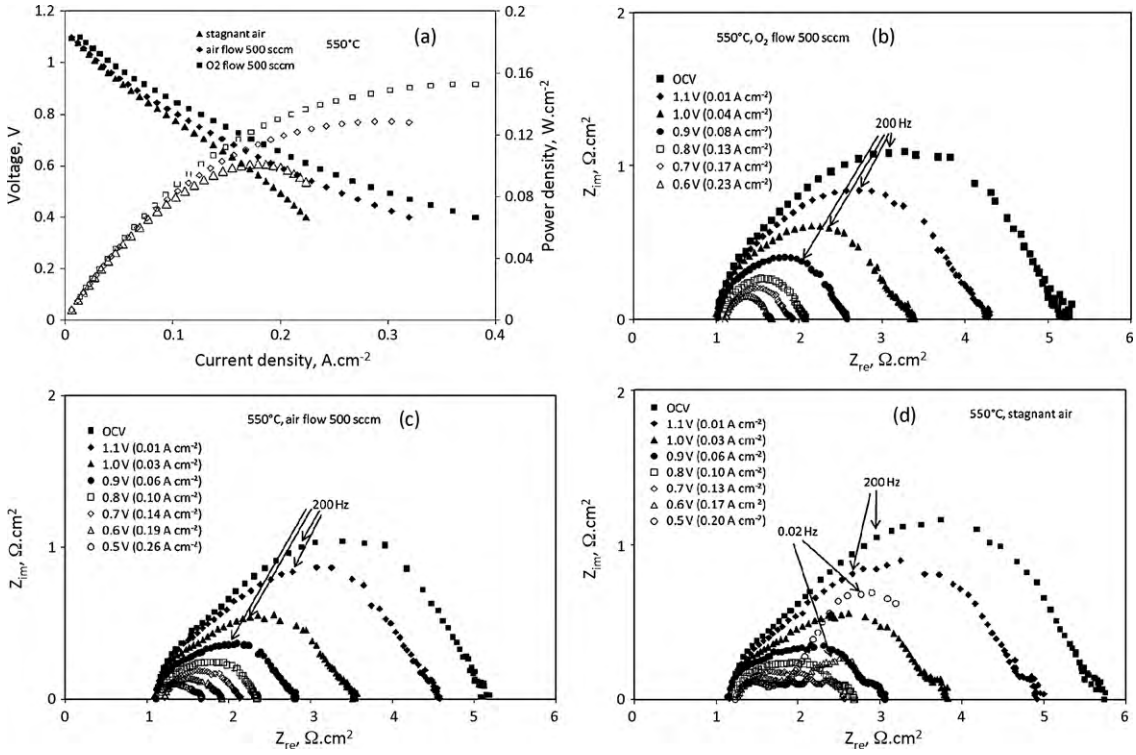

Fig. 3. *I–V* characteristics (a) and electrochemical impedance spectra (b–d) of a fuel cell tested at 550 °C in three different cathode environments.

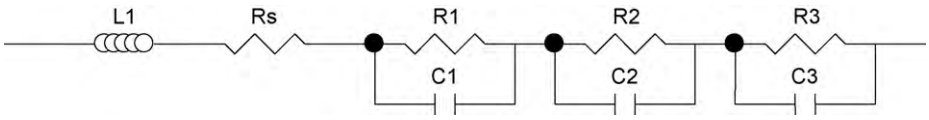

Fig. 4. Equivalent circuit used to fit the electrochemical impedance spectra in Figs. 2 and 3.

curve tested in stagnant air and flowing air showed a remarkable increase in slope when the current density exceeded a certain value, 0.4 A cm^{-2} for fuel cells in stagnant air and 0.9 A cm^{-2} in flowing air at 750 °C, with the corresponding voltages of 0.9 V and 0.8 V in the curves, respectively. Only the *I–V* curve tested in flowing oxygen did not show any turning point; instead, the slope of the curve continued to decrease as the current density increased, exhibiting a concave-up curvature.

The different behaviors of the *I–V* characteristics can be explained by the corresponding EIS, as shown in Fig. 2b–d. At OCV, all the impedance spectra measured in different cathode environments had almost the same shape and magnitude, which gave an ohmic resistance of about 0.12 Ω cm^2 and an overall polarization resistance of 0.5 Ω cm^2. All the values of the ohmic and polarization resistance from electrochemical impedance spectra in this study were obtained by fitting the impedance spectra with the equivalent circuit, shown in Fig. 4. In the circuit, L_1 represents the inductance from the wires of the testing system; R_s is the ohmic resistance of the fuel cell; R_1, R_2, R_3 stand for the polarization resistance of the arcs in the EIS, with the corresponding constant phase elements C_1, C_2, and C_3, respectively. The ohmic resistance of the cell remained almost constant as the operating voltage decreased (current density increased) for all three cathode testing environments, consistent with our previous study [6]. However, the polarization resistance of the cell behaved very differently under different cathode testing conditions as the operating voltage decreased.

In flowing oxygen, three arcs were found in the impedance spectra (Fig. 2b). Since their specific attributions were undetermined, only the overall polarization resistance was considered. The polarization resistance decreased with decreasing operating voltage (and increasing current density) over the entire range, as shown in Fig. 5. The change in polarization resistance was found to obey the Tafel equation, in which the ohmic-free over-potential (ΔV) of the cell is given by

$$\Delta V = A \ln\left(\frac{i}{i_0}\right) \quad (1)$$

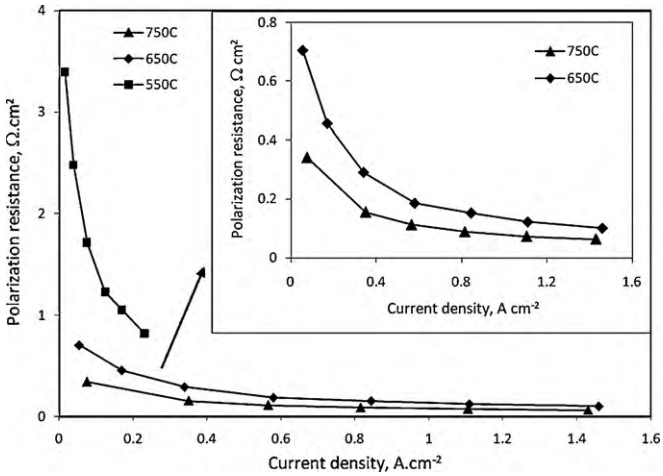

Fig. 5. Polarization resistance of a fuel cell as a function of current density in flowing 100% oxygen at different temperatures.

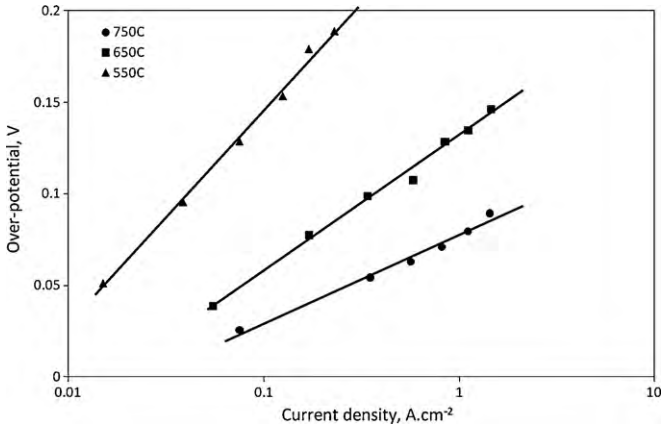

Fig. 6. Over-potential of a fuel cell as a function of the current density in flowing 100% oxygen at different temperatures.

where A is a constant (Tafel slope), i and i_0 are current density and exchange current density, respectively. Therefore, the ohmic-free over-potential of the fuel cell was plotted against the logarithm of the current density, as shown in Fig. 6. The ohmic-free over-potential was calculated as a product of the polarization resistance obtained from EIS (the sum of R_1, R_2, and R_3 in the equivalent circuit) and the corresponding current density. It is shown that at all the measuring temperatures, a logarithmic relationship between the ohmic-free over-potential and the current density was maintained. By fitting the curve, the Tafel slope and the exchange current density at different temperatures were determined, as summarized in Table 1. It can be seen that, as the temperature decreased from 750 °C to 550 °C, the Tafel slope increased from 20 mV to 50 mV, while the exchange current density decreased from 25 mA cm^{-2} to 6 mA cm^{-2}. The exchange current densities are lower than those reported by Liu et al. [18] for $La_{0.8}Sr_{0.2}Co_{0.8}Fe_{0.2}O_3$ cathodes of 65 mA cm^{-2} at 700 °C, and by Qiang et al. [19] for $La_{0.58}Sr_{0.4}Co_{0.2}Fe_{0.8}O_3 + Gd_{0.2}Ce_{0.8}O_{1.9}$ composite cathode of 301 mA cm^{-2} at 750 °C.

Since the polarization resistance from the anode reaction is usually negligible, the major contribution to the polarization resistance of the fuel cell is from the cathode reaction (oxygen reduction reaction) [20,21]. Because the Tafel equation is valid only when the electrode reaction is controlled by electrical charge transfer at the electrode (and not by the mass transfer to or from the electrode surface), the logarithmic relationship between the current density and the over-potential indicates that charge transfer is the rate-determining step of the cathode reaction for the LSCF cathode in flowing oxygen. This also means that oxygen diffusion to the surface of the cathode or the triple-phase-boundary is not a limiting step for the cathode reaction in flowing oxygen, even at high current densities when oxygen consumption is high. This is not surprising

Table 1
Tafel slopes and exchange current densities of a fuel cell measured at various temperatures in flowing oxygen.

Temperature	550 °C	650 °C	750 °C
Tafel slop	50 mV	30 mV	20 mV
Exchange current density	6 mA cm^{-2}	16 mA cm^{-2}	25 mA cm^{-2}

considering the porous nature of the LSCF cathode and the pure oxygen environment.

In flowing air, the polarization resistance also decreased with increasing current density when the current density was small, as shown in Fig. 2c. However, when the current density exceeded a certain value (in this case 0.6 A cm^{-2} at 0.9 V), a new arc appeared in the low frequency end of the spectrum and increased in size as the current density increased. The resistance of the new arc dominated the total resistance at high current densities, which was reflected by the change in slope in the *I–V* curve. This phenomenon was exaggerated in stagnant air, as shown in Fig. 2d. The new arc appeared at a much smaller current density, 0.18 A cm^{-2} in stagnant air compared to 0.6 A cm^{-2} in flowing air, and increased with the current density.

The new arc is believed to be related to the diffusion of molecular oxygen in the gas phase through the majority species (molecular nitrogen) present in the pores in the electrode layer. Similar phenomena were found for dense cathodes in air or porous cathodes at relatively low oxygen partial pressures [8,10,14,22]. However, the gas diffusion problem at the high oxygen consumption rates associated with operating at high current densities in air has not been well studied.

It has been shown that for a cathode thickness of l_c with spatially invariant porosity and tortuosity, the partial pressure of oxygen at the cathode/electrolyte interface, $p_{O_2(c)}$, is given by [23]

$$p_{O_2(c)} = p - \left(p - p^o_{O_2}\right) \exp\left[\frac{iRT\tau_c l_c}{4FD_c p V_{v(c)}}\right] \quad (2)$$

where p is the total pressure, $p^o_{O_2}$ is the invariable oxygen partial pressure outside of the cathode, i is the current density, τ_c is the tortuosity factor, D_c is the oxygen diffusion coefficient in the cathode, $V_{v(c)}$ is the volume fraction of porosity of the cathode, and F, R, and T have their regular meanings.

For an anode-supported fuel cell with small cathode thickness, the exponential part can be approximated and Eq. (2) can be written as [23]

$$p_{O_2(c)} = p^o_{O_2} - \frac{p - p^o_{O_2}}{p} \frac{RT\tau_c l_c}{4FD_c V_{v(c)}} i \quad (3)$$

Eqs. (2) and (3) imply that the presence of other gas species besides oxygen in the cathode gas stream (e.g. nitrogen, in the case of air) is the source of gas diffusion limitation in SOFC cathodes and that microstructural optimization of the cathode is important in mitigating these effects. For instance, in the flowing 100% oxygen atmosphere, since $p^o_{O_2} \approx p$, it is easy to derive that $p_{O_2(c)} \approx p^o_{O_2} \approx p$, which means that according to these equations, the oxygen partial pressure at the interface of the cathode and the electrolyte is independent of the current density. This is consistent with the impedance results in flowing oxygen (Fig. 2b) where no diffusion-related arc was observed as the current density increased. In the case of fuel cells tested in air, $p_{O_2(c)}$ decreases with the current density because $p^o_{O_2}$ is smaller than p from Eqs. (2) and (3). Since the oxygen consumption in the cathode or at the interface of the cathode and the electrolyte increases with the current density, at high current densities, a large amount of oxygen is consumed, leaving behind excessive inert nitrogen in the pores of the cathode or at the interface, which hinders the transport of oxygen to the active reaction sites in the cathode or at the interface. Therefore, a decreased oxygen partial pressure at high current densities is anticipated, consistent with Eq. (3). It is reported that polarization resistance has a simple inverse relationship with the oxygen partial pressure if the rate-determining step involves the diffusion of molecular oxygen [13,24]. Therefore, as the current density increases, the oxygen partial pressure at the interface of the cathode and the electrolyte decreases, resulting in an increase in the electrode resistance.

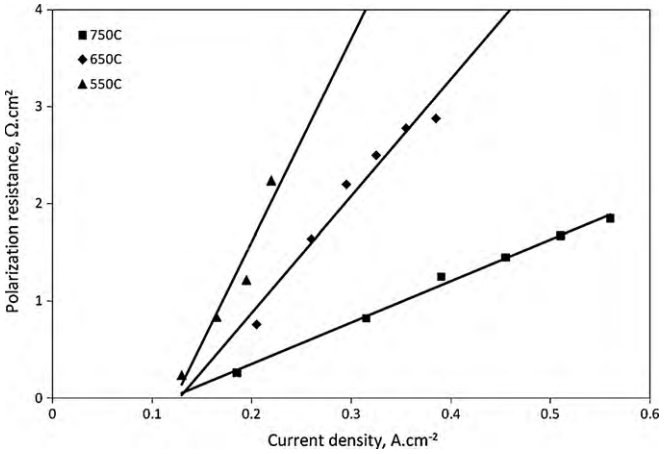

Fig. 7. Plot of the concentration polarization resistance of a fuel cell with current density in stagnant air at different temperatures.

The concentration polarization resistance related to the oxygen diffusion at different temperatures was plotted as a function of the current density, as shown in Fig. 7. The concentration polarization resistance was obtained from the resistance of the new arc appearing at the low frequency end of the EIS measured at high current densities in stagnant air at different temperatures. A linear relationship was found between the concentration polarization resistance and the current density at all the measuring temperatures. By fitting the results linearly, the slope and the intercept of the lines with the x axis can be obtained. The slope of the lines decreased with increasing temperature, while the intercept with the x axis remained constant. The slope of the line indicates how fast the polarization resistance increases with the current density, while the intercept with the x axis indicates when the polarization resistance starts to contribute to the total resistance (threshold current density). According to the Chapman–Enskog theory [25], the diffusion coefficient of a gas is proportional to $T^{3/2}$. If this $T^{3/2}$ dependence is substituted for D_c in Eq. (3), it is easily derived that the slope of $p_{O_2(c)}$ as a function of current density is proportional to $-T^{-1/2}$, meaning that at higher temperatures, the oxygen partial pressure at the interface will be depleted more slowly with increasing current density than at lower temperatures. Because concentration polarization is the direct result of oxygen depletion, this explains the decreasing slope with increasing temperature observed in Fig. 7. The fact that the threshold current density is independent of the measuring temperature further strengthens the argument that this resistance is related to the oxygen consumption rate, which is only dependent on the current density.

As the testing temperature decreased to 550 °C, the power density of the fuel cell decreased dramatically, as well as the difference in cell performance between different cathode environments. The maximum power densities were 0.10 W cm^{-2}, 0.13 W cm^{-2}, and 0.15 W cm^{-2} in stagnant air, flowing air, and flowing oxygen, respectively. Only a 50% increase in power density was observed at 550 °C when the cathode environment changed from stagnant air to flowing oxygen, while a 4-fold increase was observed at 750 °C.

The decrease in power density was due to an increase in both ohmic and polarization resistance of the fuel cell as the temperature decreased, indicated in the corresponding EIS (Fig. 3b–d). Because of the low current density and therefore low oxygen consumption rate at this temperature, concentration polarization did not influence the power density as much as it did at 750 °C. At 550 °C, only the fuel cell tested in stagnant air showed a distinguishable slope change at a current density of 0.16 A cm^{-2} with corresponding voltage of 0.6 V, where the resistance of the diffusion-related arc made a significant contribution to the total resistance (Fig. 3d).

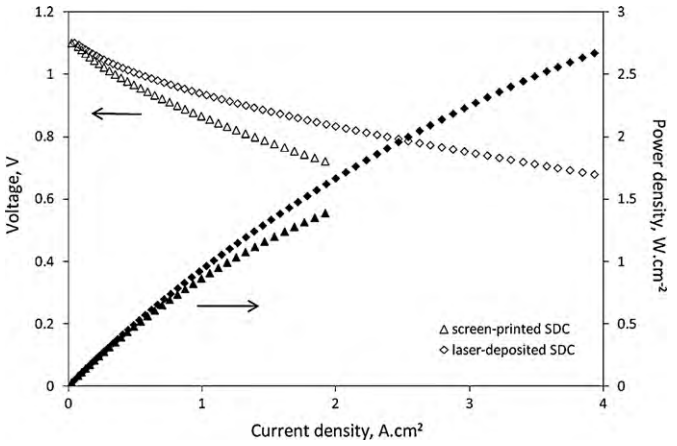

Fig. 8. *I–V* characteristics of fuel cells with screen-printed SDC and laser-deposited SDC interlayer in flowing oxygen at 750 °C.

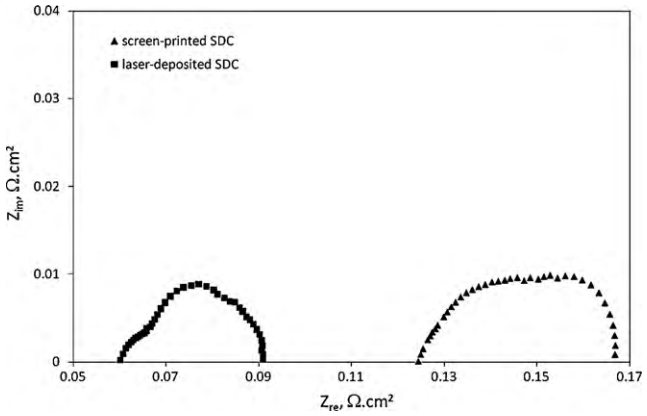

Fig. 9. Electrochemical impedance spectra (measured at 0.8 V) of fuel cells with screen-printed SDC and laser-deposited SDC in flowing oxygen at 750 °C.

3.3. Effect of ohmic and polarization resistance on cell performance

In our previous study [6], as well as in this one, it has been shown that the polarization resistance of a fuel cell is a dynamic property, which changes with the current density of the fuel cell. Therefore, performance evaluation of the cell components based on the data obtained at OCV may be inaccurate or even misleading. For example, at 750 °C, from the electrochemical impedance spectroscopy performed at OCV (Fig. 2b–d), the ohmic and polarization resistances were 0.12 Ω cm^2 and 0.50 Ω cm^2, respectively. Assuming that the polarization resistance of the anode is very small and can be neglected, it seems that the polarization resistance of the cathode dominates the total resistance due to its insufficient electrocatalytic activity. However, as this study has shown, in flowing oxygen where concentration polarization can be eliminated, the polarization resistance decreases significantly as the current density increases. At a current density of 1.4 A cm^{-2} (corresponding voltage 0.8 V), the polarization resistance is only 0.05 Ω cm^2, compared to the invariable ohmic resistance 0.12 Ω cm^2. Therefore, efforts should be made to decrease the ohmic resistance of the fuel cell, instead of further reducing the polarization resistance of the cathode, usually by identifying better cathode materials or improving the existing cathode material. The reason that the polarization resistance of the cathode in flowing oxygen is considered is because it is free of concentration polarization. Similar polarization resistance should be anticipated in air if the microstructure of the cathode can be optimized so that the concentration polarization can be negligible. From this perspective, we prepared a fuel cell with a pulsed-laser-deposited (PLD) SDC interlayer, which proved to have a smaller ohmic resistance than the fuel cells with a conventional screen-printed SDC interlayer [17].

Figs. 8 and 9 show the *I–V* characteristics of the fuel cell with the PLD SDC interlayer and the electrochemical impedance spectra performed at 0.8 V, respectively, at 750 °C in pure oxygen flowing at a rate of 500 sccm. Also included in the figures are results for a fuel cell with a conventional screen-printed SDC interlayer tested in pure oxygen flow for comparison. A power density of 2.6 W cm^{-2} was achieved at 0.7 V for the fuel cell with a PLD SDC interlayer. Similar high power density was also achieved by Yan et al. on an anode-supported, laser-deposited $La_{0.8}Sr_{0.2}Ga_{0.8}Mg_{0.2}O_3$ electrolyte fuel cell tested in pure oxygen [26]. The extraordinarily high power density of the fuel cell was due to low ohmic and polarization resistances of the fuel cell, indicated by the impedance spectroscopy performed at 0.8 V (Fig. 9). The ohmic and polarization resistances were 0.06 Ω cm^2 and 0.03 Ω cm^2, respectively at 750 °C in flowing oxygen, while those for the fuel cell with a conventional screen-printed SDC interlayer were 0.12 Ω cm^2 and 0.04 Ω cm^2, respectively. The decrease in ohmic resistance was partially attributed to the dense SDC interlayer with improved electrical conductivity and good bonding between the SDC interlayer and the YSZ electrolyte. The very small polarization resistance means that LSCF is a satisfactory cathode material for intermediate temperature SOFC applications.

Another implication from the extraordinarily high performance of the fuel cells in flowing oxygen where concentration polarization is eliminated is that, even for a "normally functional" fuel cell in air, concentration polarization still dominates the total cell resistance at high current densities, limiting the cell performance. Optimization of the microstructure of the cathode or employment of new cathode design which can mitigate the oxygen difussion problem might enhance the cell performance significantly. Recently, numerical modeling by several groups [27–30] proposed that by changing the microstructure of the electrode, improved performance can be expected. Ni et al. [27] found that for a composite cathode with 40% (volume) porosity, diffusion limitation can be expected even in air if the electrode particle size decreases below 0.2–0.3 μm. An innovative thin-walled geometry proposed by Ramakrishna et al. [29] showed an improved cell performance compared to the plain one due to the better distribution of reactants along the length in the thin-walled geometry.

4. Conclusion

Anode-supported fuel cells were tested in three different cathode environments: stagnant air, flowing air, and flowing oxygen at temperatures from 550 °C to 750 °C. Electrochemical impedance spectroscopy performed under a series of operating voltages revealed features which have not been well documented. In flowing oxygen, the polarization resistance decreased considerably with the current density. The ohmic-free over-potential of the fuel cell calculated from the polarization resistance and the corresponding current density showed a linear relationship with the logarithm of the current density. In air, an additional arc related to diffusion of molecular oxygen arose in the low frequency end of the spectrum at high current densities and increased in size as the current density was further increased due to the low oxygen partial pressure at the interface of cathode and the electrolyte. Optimization of the microstructure of the cathode or employment of a new cathode design which can mitigate the oxygen diffusion problem might enhance cell performance significantly.

Acknowledgement

This work was supported by the US Department of Energy's Solid-state Energy Conversion Alliance Core Technology Program. The authors would like to thank Daniel Fisher at the University of Houston for preparation of the dense SDC interlayer by pulsed laser deposition.

References

[1] S.B. Adler, Chem. Rev. 104 (2004) 4791.
[2] E.V. Tsipis, V.V. Kharton, J. Solid State Electr. 12 (2008) 1367.
[3] E.C. Thomsen, G.W. Coffey, L.R. Pederson, O.A. Marina, J. Power Sources 191 (2009) 217.
[4] J.R. Smith, A. Chen, D. Gostovic, D. Hickey, D. Kundinger, K.L. Duncan, R.T. DeHoff, K.S. Jones, E.D. Wachsman, Solid State Ionics 180 (2009) 90.
[5] E.P. Murray, M.J. Sever, S.A. Barnett, Solid State Ionics 148 (2002) 27.
[6] X.D. Zhou, L.R. Pederson, J.W. Templeton, J.W. Stevenson, J. Electrochem. Soc. 157 (2010) B220.
[7] S. McIntosh, S.B. Adler, J.M. Vohs, R.J. Gorte, Electrochem. Solid State 7 (2004) A111.
[8] N. Grunbaum, L. Dessemond, J. Fouletier, F. Prado, L. Mogni, A. Caneiro, Solid State Ionics 180 (2009) 1448.
[9] V.C. Kournoutis, F. Tietz, S. Bebelis, Fuel Cells 9 (2009) 852.
[10] S.B. Adler, J.A. Lane, B.C.H. Steele, J. Electrochem. Soc. 143 (1996) 3554.
[11] J.D. Kim, G.D. Kim, J.W. Moon, Y. Park, H.W. Le, K. Kobayashi, M. Nagai, C.E. Kim, Solid State Ionics 144 (2001) 387.
[12] S. Bebelis, N. Kotsionopoulos, A. Mai, F. Tietz, J. Appl. Electrochem. 37 (2007) 15.
[13] A. Ringuede, J. Fouletier, Solid State Ionics 139 (2001) 167.
[14] A. Endo, M. Ihara, H. Komiyama, K. Yamada, Solid State Ionics 86–88 (1996) 1191.
[15] W.S. Wang, M.D. Gross, J.M. Vohs, R.J. Gorte, J. Electrochem. Soc. 154 (2007) B439.
[16] S.P. Simner, M.D. Anderson, L.R. Pederson, J.W. Stevenson, J. Electrochem. Soc. 152 (2005) A1851.
[17] Z.G. Lu, X.D. Zhou, D. Fisher, J. Templeton, J. Stevenson, N.J. Wu, A. Ignatiev, Electrochem. Commun. 12 (2010) 179.
[18] J.B. Liu, A.C. Co, S. Paulson, V.I. Birss, Solid State Ionics 177 (2006) 377.
[19] F. Qiang, K.N. Sun, N.Q. Zhang, X.D. Zhu, S.R. Le, D.R. Zhou, J. Power Sources 168 (2007) 338.
[20] K.J. Yoon, S. Gopalan, U.B. Pal, J. Electrochem. Soc. 155 (2008) B610.
[21] H.M. Xiao, T.L. Reitz, M.A. Rottmayer, J. Power Sources 183 (2008) 49.
[22] D. Gostovic, J.R. Smith, D.P. Kundinger, K.S. Jones, E.D. Wachsman, Electrochem. Solid State 10 (2007) B214.
[23] J.W. Kim, A.V. Virkar, K.Z. Fung, K. Mehta, S.C. Singhal, J. Electrochem. Soc. 146 (1999) 69.
[24] S.B. Adler, Solid State Ionics 111 (1998) 125.
[25] S. Chapman, T.G. Cowling, The Mathematical Theory of Non-Uniform Gases, 3rd ed., Cambridge University Press, 1970 [Chapters 10 and 14].
[26] J.W. Yan, H. Matsumoto, M. Enoki, T. Ishihara, Electrochem. Solid State 8 (2005) A389.
[27] M. Ni, M.K.H. Leung, D.Y.C. Leung, J. Power Sources 168 (2007) 369.
[28] J.J. Hwang, C.K. Chen, D.Y. Lai, J. Power Sources 143 (2005) 75.
[29] P.A. Ramakrishna, S. Yang, C.H. Sohn, J. Power Sources 158 (2006) 378.
[30] Y.H. Koh, J.J. Sun, W.Y. Choi, H.E. Kim, J. Power Sources 161 (2006) 1023.